In vivo application of an implantable tri-anchored methylene blue-based electrochemical pH sensor

In vivo application of an implantable tri-anchored methylene blue-based electrochemical pH sensor

Eva González-Fernández,[a§] Matteo Staderini,[a§] Jamie R. K. Marland,[b] Mark E. Gray,[c] Ahmet Uçar,[a,d] Camelia Dunare,[b] Ewen O. Blair,[b] Paul Sullivan,[d] Andreas Tsiamis,[d] Stephen N. Greenhalgh,[c] Rachael Gregson,[c] Richard Eddie Clutton,[c] Stewart Smith,[d] Jonathan G. Terry,[b] David J. Argyle,[c] Anthony J. Walton,[b] Andrew R. Mount,[a*], Mark Bradley[a*], Alan F. Murray.[d*]

[a] *EaStCHEM, School of Chemistry, University of Edinburgh, Joseph Black Building, West Mains Road, Edinburgh, EH9 3FJ, UK.*

[b]*School of Engineering, Institute for Integrated Micro and Nano Systems, University of Edinburgh, Scottish Microelectronics Centre, The King's Buildings, Edinburgh, EH9 3FF, UK.*

[c]*The Royal (Dick) School of Veterinary Studies and Roslin Institute, University of Edinburgh, Easter Bush, Roslin, Midlothian, EH25 9RG, UK.*

[d] *School of Engineering, Institute for Bioengineering, University of Edinburgh, Faraday Building, The King's Buildings, Edinburgh EH9 3DW, UK.*

[§]These authors contributed equally to this study

*Corresponding authors. Fax: +44 131 777 0334

E-mail: mark.bradley@ed.ac.uk; a.mount@ed.ac.uk; alan.murray@ed.ac.uk

Abstract

The development of robust implantable sensors is important in the successful advancement of personalised medicine as they have the potential to provide *in situ* real-time data regarding the status of health and disease and the effectiveness of treatment. Tissue pH is a key physiological parameter and herein, we report the design, fabrication, functionalisation, encapsulation and protection of a miniaturised self-contained electrochemical pH sensor system and characterisation of sensor performance. Notably for the first time in this environment the pH sensor was based on a methylene blue redox reporter which showed

remarkable robustness and accuracy and sensitivity. This was achieved by encapsulation of a self-assembled monolayer containing methylene blue entrapped within a Nafion layer. Another powerful feature was the incorporation, within the same implanted device, of a fabricated on-chip Ag/AgCl reference electrode – vital in any electrochemical sensor, but often ignored. When utilised *in vivo*, the sensor allowed accurate tracking of externally induced pH changes within a naturally occurring ovine lung cancer model, and correlated well with single point laboratory measurements made on extracted arterial blood, whilst enabling *in vivo* time-dependent measurements. The sensors functioned robustly whilst implanted, and maintained *in vitro* function once extracted and together, these results demonstrate proof-of-concept of the ability to sense real-time intratumoral tissue pH changes *in vivo.*

Keywords: Implantable, sensor, pH, methylene blue, tumour, microfabrication.

1. Introduction

Advancing the development of implantable sensing technologies is a key focus in the medical device field (Gray et al., 2018; Scholten and Meng, 2018; Inmann and Hodgins, 2013). This multidisciplinary field, which involves engineers, chemists and biomedical scientists, amongst others, is linked to providing the data which underpins and informs the development of personalised/precision medicine, with the aim of developing miniaturised, accurate, reliable and safe implantable devices.

Implantable sensors are within the category of “active implantable medical devices”, which differentiates them from other implanted medical devices that are not designed to perform an active task, such as a hip implant or a stent. Active implantable medical devices include pacemakers (Verma and Knight, 2019), cochlear implants (Wilson et al., 1991) infusion pumps (Cobo et al., 2016) or neuro stimulators (Edwards et al., 2017). Current available implanted medical devices with sensing capabilities are limited to continuous glucose monitoring, with the FDA approving the first implantable glucose monitoring system in 2018 (Eversense® XL). This is constructed around a subcutaneously implanted device with fluorescence-based detection and readout which uses a removable and rechargeable transmitter.

Electrochemical-based strategies have long been at the forefront of the development of portable and miniaturised sensing technologies (Gu et al., 2018; Terry et al., 2013) and are well positioned to play an important role in the field of implantable medical devices, particularly given their ease of miniaturisation and the progress made in coupling them to advanced technologies such as complementary metal-oxide semiconductor (CMOS) integrated circuits (Giagkoulovits et al., 2018). This offers the possibility of developing stand-alone devices that combine the ability to support the embedding of electrochemical components such as electrodes, which can then be specifically chemically modified for selectivity to the target analyte(s) of interest, with their ability to transduce the response into electrical signals as ideal input/output signals for recording measurements and enabling analysis.

The availability of technologies that allow continuous local monitoring of diagnostic physiological parameters including O_2, CO_2, pH and/or ions such as Na^+ or K^+ would support an evolution in the clinical management of different diseases, with the resulting information potentially paving the way to more personalised treatments. Enormous advances are being made in these areas with the development, for instance of miniaturised electrochemical oxygen sensors which have been successfully implanted for measuring intestinal oxygen levels in rats (Gray et al., 2019) and lung tumour oxygenation levels in sheep (Marland et al., 2020) and the fiber-based implantable sensor that has allowed electrochemical monitoring of H_2O_2 in solid tumours (Wang et al., 2020). pH is a key physiological parameter which indicates the health and local state of a given tissue for a range of diseases. This is particularly true for cancer, where tissue acidity has been identified as an important marker (Swietach et al., 2014). Continuous knowledge/measurement of local tissue pH would therefore expand the understanding of biological processes associated to such diseases. Image-based techniques for pH measurement have been reported using a variety of techniques such as magnetic resonance imaging (MRI) (Gallagher et al., 2008), fluorescence imaging coupled to fiber-optics (Choudhary et al., 2019), and even hydrogel swelling linked to a radiography readout (Arifuzzaman et al., 2019). Electrochemical-based methods have also been explored, such as iridium oxide-based potentiometric devices used to measure pH in a rat's brain undergoing an ischaemic insult (stroke) (Grant et al., 2001), a hydrogen selective carbon nanotube-modified micro needle potentiometric sensor used for *in vivo* transdermal pH monitoring (García-Guzmán et al., 2021), or ion-sensitive field-effect transistor (ISFET) technology, which has attracted much attention over recent years in the area of pH sensing (Hammond et al, 2004; Nakata et al., 2017; Douthwaite et al., 2017). However, there is still a challenge in producing appropriately miniaturised, stable, sensitive, robust, and quantitative pH sensor systems capable of long-term implantation.

The fabrication of electroactive films on an electrode surface is common practice in the development of different selective electrochemical sensors. Various redox reporters or mediators have also been extensively used, such as ferrocene (Rudnev et al., 2013) or

methylene blue (MB) (Kelley et al, 1997; González-Fernández et al., 2018), either in solution or anchored on the electrode surface as monolayers. MB in particular is a pH-sensitive redox reporter, which due to the involvement of protons in its redox reaction also shows changes in its redox potential with pH in solution (Koutsoumpeli et al., 2015).

In this work we exploit this feature by fabricating and characterising a miniaturised electrochemical pH sensor which employs a pH-sensitive MB-based self-assembled monolayer (SAM) on an electrode surface. The sensor fabrication and response was first characterised *in vitro* using commercial screen-printed gold electrodes (SPAuEs) and then the procedure was subsequently adapted for use on in-house Pt microfabricated devices, using technology consistent with their incorporation into implantable sensing systems. These were characterised and successfully driven and validated *in vivo* as a proof-of-concept demonstration of the ability to measure real-time intratumoural pH changes in a naturally occurring ovine lung cancer model.

2 Materials and methods

The detailed experimental procedures are described in the Supplementary Information and include:

2.1. Synthesis of the pH sensitive probes
2.2. Microfabrication of silicon-based Pt devices
2.3. Packaging of the silicon-based Pt devices
2.4. In-house silicon-based Pt device modification
2.5. SPAuE modification
2.6. Integrity of Nafion membrane assessment.
***2.7. In vitro* electrochemical measurements for characterisation.**
2.8. Sensor sterilisation and radiation.
2.9. Sensor implantation.

2.10. *In vivo* electrochemical measurements

To assess the ability of the implanted sensors to detect changes in intratumoural pH, protocols were devised that would induce changes in arterial blood pH. Respiratory acidosis

was achieved through the administration of up to 6% CO_2 in the inspired gas mixture; whereas a respiratory alkalosis was achieved by mechanical lung hyperventilation. Each procedure step was performed for approximately 15 min with a recovery period of approximately 10 min between interventions to allow blood pH to return to baseline levels (exact timings varied slightly according to the achieved blood pH measurement). Arterial blood samples were taken at the start, intermittently throughout the interventions and at the end of each procedure. The implanted devices (100 µm diameter Pt single working electrode, unless otherwise stated) were driven using a portable potentiostat (EmStat3 Blue potentiostat, Palmsens BV). Immediately prior to implantation the status of the fully integrated and packaged miniaturised pH sensors were checked by measuring the open circuit potential (OCP) value of the on-chip, solid state Ag/AgCl/Nafion RE versus an external Ag | AgCl | Cl^- (3 M) and by running a single SWV in PBS. Once implanted, SWV was performed continuously in the potential window 0 to −0.4 V vs on-chip reference electrode with a step potential of 5 mV, 25 mV of amplitude and 60 Hz frequency. Both forward (from –0.4 V to 0 V) and reverse (0 V to -0.4 V) SWV were recorded sequentially. Peak potentials for the registered voltammograms were plotted with time and subsequently intratumoural pH values were calculated employing pre-implantation calibration graphs registered *in vitro*. A calculated pH value is estimated from both forward and reverse processes and averaged to get the final sensor output.

3. Results and discussion

3.1. Sensor fabrication and characterisation on SPAUEs

MB (**1**) is a reversible redox reporter that can be reduced and reoxidised at an electrode surface through an electrochemically reversible 2 e^-/ n H^+ process to give leuco-methylene blue, (LMB (**2**)) (Ju et al., 1995). The number of protons involved in this process can vary from 1 to 2, depending on the pH relative to the pK_a for the second protonation step of LMB , with a 2 e^-, 1 H^+ exchange for neutral to basic pHs where pH > pK_a, whereas 2 e^- /2 H^+

reduction has been reported under acidic conditions to give $[MBH_2]^+$ (LMB^+ (**3**)) where pH < pK_a (Fig. 1A) (Ju et al., 1995).

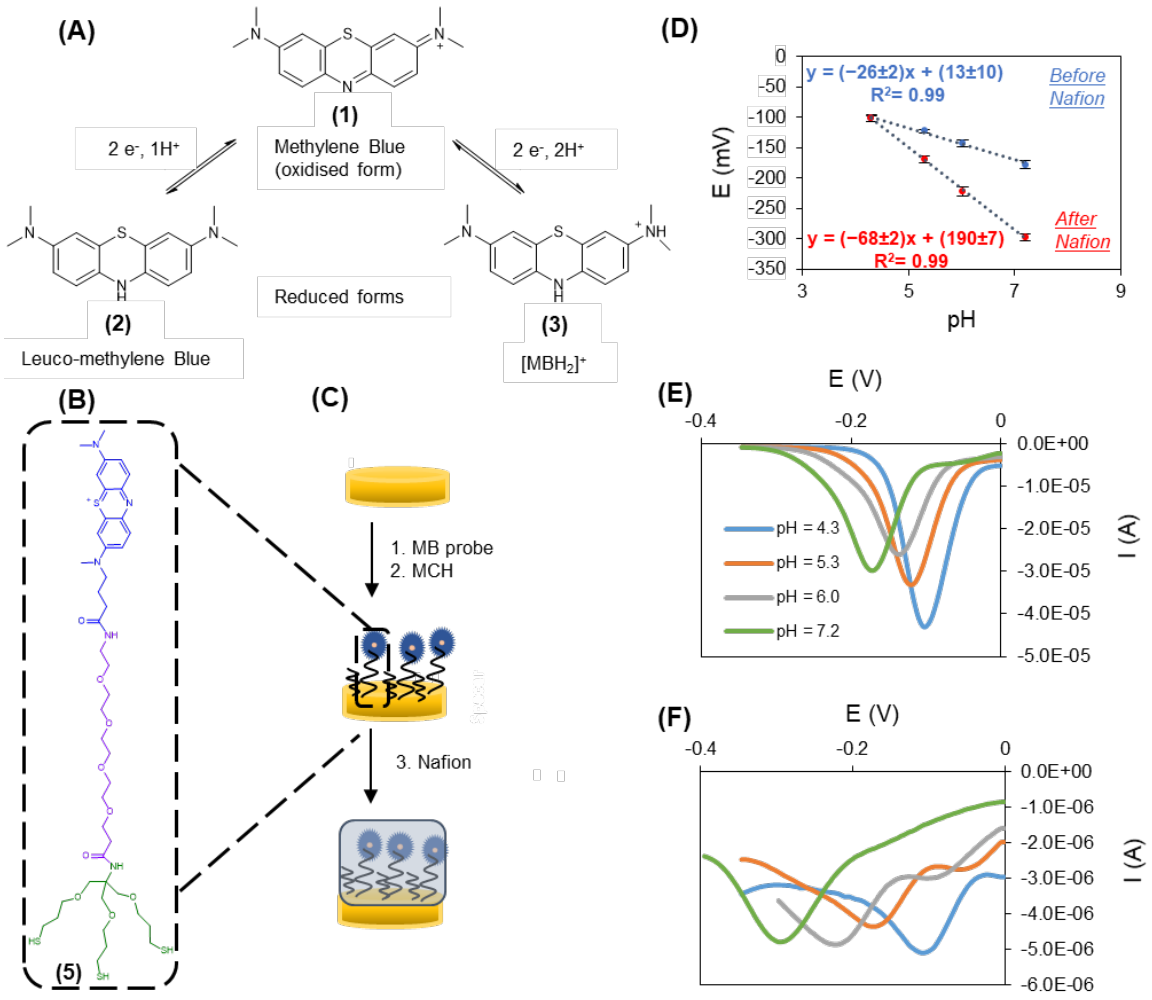

Figure 1. Electrochemical pH sensor. Principle of detection. (A) Redox processes for methylene blue (**1**) at different pH ranges to give leuco-methylene blue (**2**) and protonated leuco-methylene blue, $[MBH_2]^+$ (**3**). (B) Chemical structure for the tripod-MB probe (**5**), consisting of a tri-branched thiol anchor (green) linked to a 4-unit ethylene glycol moiety (purple) which connects to the pH-sensitive MB reporter (blue). (C) Preparation of the sensing phase using SPAuEs consisting of the formation of a mixed SAM of the selected methylene blue probe (single-branched-MB or tri-branched-MB) and mercaptohexanol and followed by drop-casting a Nafion layer from a (1 : 3) Nafion : water mixture. (D) Variation of methylene blue peak potentials measured by SWV for t-MB/SPAuEs (blue circles) and Nafion/t-MB/SPAuEs (red circles) versus the pH of varying phosphate buffered solutions in the range

of 4–7.4. All data points represent the average and standard deviation for 4 individual sensing phases and straight lines correspond to the linear fits. (E) Overlay of square wave voltammograms registered before and (F) after Nafion layer formation for a t-MB/SPAuE immersed in phosphate buffered solutions with varying pH values: pH=4.3 (blue line); pH=5.3 (orange line); pH=6 (grey line) and pH=7.2 (green line).

In this work, MB was chemically modified in order to provide a substituent thiol-terminated group as a means for immobilisation onto a gold electrode, through the formation of a SAM through the thiol-Au interaction (Love et al., 2005). An ethylene glycol spacer was also introduced between the MB and the thiol anchor to confer hydrophilicity and flexibility, thereby ensuring a solution-like environment and efficient electron transfer at the electrode surface. Two probes were synthesised, one containing a single thiol group, s-MB ((**4**) Supplementary Fig. 1) and the other tri-branched with three thiol groups, t-MB (**5**) (Fig. 1B), designed to confer enhanced SAM film formation and stability (Staderini et al., 2018). The construction of the sensing layer on the electrode surface then consisted of two steps: formation of a SAM of the selected probe (s-MB or t-MB) followed by deposition of a Nafion polymer protective layer (Fig. 1C). The MB-containing probes were first immobilised on SPAuEs as SAMs, and the SAM-modified SPAuEs were subjected to SWV measurements in phosphate buffer with varying pH values in the range of 4–8. Both s-MB (Supplementary Fig. 2) and t-MB (Fig. 1D) SAMs showed a linear dependency of the SWV peak potential for the MB reduction on pH, with a slope of −27±3 mV/pH and −26±2 mV/pH at room temperature, respectively, which corresponds well within error to the expected linear Nerstian behaviour for a 2 e^- / 1 H^+ redox process (with a theoretical slope of −30 mV/pH). The pH-responsive SAM was then covered with the Nafion polymer membrane by drop casting, which acts as a physical protective layer for the active sensing SAM against

biofouling from the complex tissue environment following implantation. Nafion is a negatively-charged perfluorinated polymeric material widely used as a cation-exchange membrane. It is also a common material used in the fabrication and integration of biosensing technologies (Tsai et al., 2005; Gong et al., 2017; Ju et al., 1995b), which has recently been shown to have good intratumoural biocompatibility when implanted into a human breast cancer xenograft tumour (Gray et al., 2019c). The effect of the Nafion coating on the pH sensing ability of the modified-SPAuEs was then evaluated by performing SWV measurements in phosphate solutions and plotting the resulting peak potentials as a function of pH. As shown in Fig. 1D and Supplementary Fig. 2, both Nafion/s-MB and Nafion/t-MB-modified SPAuEs were pH-responsive. Interestingly, the Nafion coating resulted in an approximately two-fold increase in the observed slope at −56±4 mV/pH and −68±2 mV/pH for the Nafion/s-MB and Nafion/t-MB sensors respectively. We hypothesise that this increase in sensitivity is attributable to the highly negatively charged Nafion backbone increasing the pK_a of LMB sufficiently through stabilising the protonated LMB^+ cation, resulting in the 2 e^- / 2 H^+ redox process and a theoretical −60 mV/pH slope under these conditions. This means that the Nafion-coated sensors exhibit a higher sensitivity against pH than their non-modified counterparts for both s-MB and t-MB probes. A typical example of the effect of the Nafion coating on the resulting SWV currents for t-MB is shown in Fig. 1E and 1F. As it is obvious from the comparison of the signals before and after the polymer was drop-casted, the Nafion layer not only causes a shift in SWV peak potential but also in peak intensity, which dropped 4-fold from 20 to 5 μA. This can be explained by the fact that the surface Nafion film could decrease the active proportion of redox SAM through only enabling electron transfer for the proportion of SAM redox molecules effectively connected through Nafion pores to the analyte solution. The effectiveness of the Nafion-coating step of the t-MB/SPAuEs was also confirmed by performing CV in PBS solution containing ferrocyanide ($Fe(CN)_6^{4-}$), a negatively charged redox probe, before and after the Nafion drop-casting step (Supplementary Fig. 3). It was reassuring that cyclic voltammograms performed on just the t-

MB SAM showed the characteristic redox process for ferrocyanide oxidation. Conversely, after Nafion coating, the resulting CV showed no redox peaks for ferrocyanide, consistent with its complete electrostatically exclusion from the Nafion film and verifying the presence of an effective Nafion coating barrier.

Nafion/t-MB was then selected as the most promising sensing layer, as the tri-branched anchor was observed to greatly improve the stability of the SAM, which is an essential attribute for implantable sensors, with their requirement for long operational times. It is also clear from Fig. 1D and Supplementary Fig. 2 that t-MB gave better performance when compared to s-MB in terms of reproducibility, for both Nafion- and non-Nafion coated sensors, which probably indicates a more reproducible and robust SAM formation. The good repeatability for Nafion/t-MB/SPAuEs, was demonstrated for 3 individual sensors by successively immersing them in solutions at two different pH values (pH 6.0 and 7.2) for a total of 20 measurements (Supplementary Fig. 4). The resulting coefficients of variation (CoV) for these measurements were 2.2% and 1.3% for pH 7.2 and 6.0, respectively. The reproducibility for multiple measurements was then confirmed by immersing the Nafion/t-MB/SPAuEs in solutions at 3 different pH values (5.7, 6.1 and 7.2) and registering 20 successive measurements within 30 min, which resulted in CoVs within 1.5% for all 3 solutions (Supplementary Fig. 5).

To evaluate their suitability for implantation purposes, for which a device sterilisation step would be required, the performance of Nafion/t-MB/SPAuE pH sensors was assessed after being subjected to a standard 24 h ethylene oxide sterilisation process. It was reassuring that this sterilisation treatment did not substantially affect the performance of the sensors in the clinically relevant pH range tested (4.3–7.2) (Supplementary Fig. 6). Nafion/t-MB/SPAuEs sensors were also found to maintain their performance after exposure to radiation (4 x 6 Gy) (Supplementary Fig. 7). This is an important outcome, as it opens up the possibility of sensor implantation into an organ/tissue likely to be treated with radiation, such as in the treatment of cancer. Assessment of the integrity of the Nafion layer after radiation

experiments also showed no changes in its ability to exclude negatively charged ions in solution (Supplementary Fig. 8).

3.2. Sensor fabrication and characterisation on in-house devices

The sensing layer developed, optimised and characterised on the SPAuE platform was then transferred to in-house microfabricated 100 μm-diameter Pt devices containing a complete miniature three-electrode cell with a Ag/AgCl reference electrode, Fig. 2A and 2B(i). Direct application of the established modification protocol for the SPAuEs did not produce fully functional devices, as there was no visible redox process corresponding to the reduction of methylene blue for solutions with a pH higher than 6 (Supplementary Fig. 9). However, this lack of activity for these 100 μm-diameter Pt based sensors was overcome by changing the surface to gold, and increasing both the active surface and roughness of the working electrode by electrochemically plating gold nanostructures, following a previously described protocol (Stine, 2019). The success of this gold plating step was confirmed by recording the characteristic cyclic voltammogram in 0.1 M H_2SO_4 for gold, in contrast to the one registered before the plating step characteristic of the Pt working electrode (Supplementary Fig. 10). A SAM of t-MB was then formed overnight on the gold-nanostructured Pt 100 μm-diameter electrode, t-MB/Au/Pt. Afterwards, a temporary protective photoresist layer covering both on-chip reference (RE) and counter (CE) electrodes was removed by rinsing with acetone and IPA (Section 2.4). The photoresist stripping protocol using mercaptohexanol-containing acetone was developed and optimised specifically for this application, as performing an established longer cleaning step (1 min) with acetone followed by immersion for 30 s in IPA resulted in a complete deactivation of the t-MB SAM layer as evidenced by the loss of redox activity (Supplementary Fig. 11). We attribute this effect to competitive adsorption and deposition of the photoresist on the t-MB-modified surface electrode, as a similar acetone treatment in the absence of the resist layer did not deactivate the redox activity of the SAM (Supplementary Fig. 12). Addition of mercaptohexanol to the acetone during rinsing proved efficient in preventing the adsorption of the photoresist onto the sensing surface, resulting in

an active surface that showed electrochemistry corresponding to the methylene blue both before and after the deposition of the Nafion layer (Supplementary Fig. 13). We hypothesise this is due to a competition step established between the mercaptohexanol and the solubilised photoresist to get adsorbed onto the surface, with the mercatohexanol binding faster and stronger leading to the preservation of an active redox surface. Finally, Nafion was drop-cast on the sensor surface as before, to improve biocompatibility and resistance to biofouling, Fig 2B(ii).

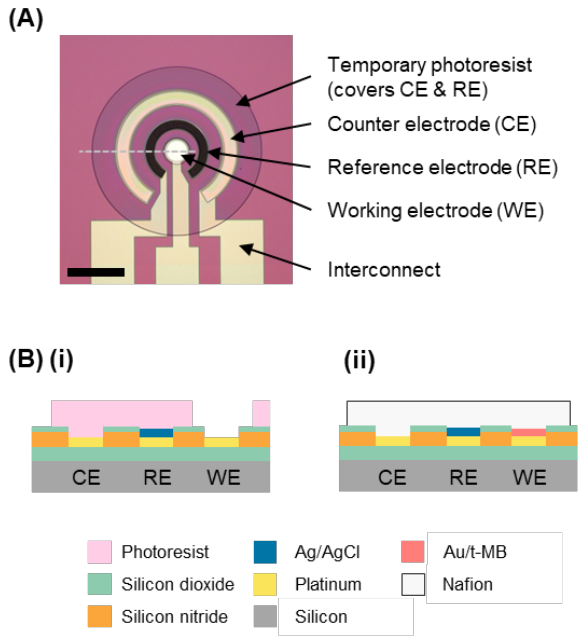

Figure 2. In-house microfabricated devices. (A) Miniature microfabricated three electrode cell prior to functionalisation, showing platinum WE (inner disc), CE (outer ring), and a Ag/AgCl RE (middle ring). The CE and RE are covered in a layer of protective photoresist leaving the WE exposed. Dashed grey line indicates position of cross-section. Scale bar shows 250 µm. (B) Schematic cross-section (not to scale) showing microfabricated electrodes (i) prior to functionalisation, and (ii) after functionalisation.

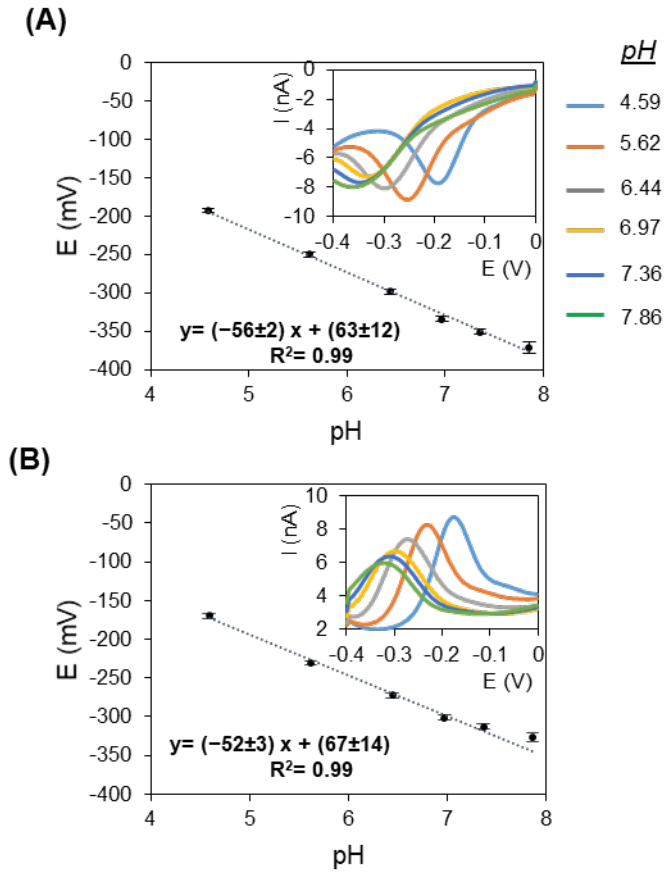

Figure 3. Calibration lines for in-house electrochemical pH sensor system. (A) Plot of the peak potentials for the reverse SWV registered with fully integrated in-house Nafion/t-MB/Au/Pt sensor system versus the pH of the phosphate buffered solution. (B) Shows the same plot corresponding to the forward SWV peak potentials. All points correspond to an average and standard deviation for 3 individual miniaturised sensors and straight lines correspond to linear fits (Note: for (B) linear regression is calculated without the point at pH=7.86, as it is clearly off the line). Insets: Square wave voltammograms registered for different phosphate buffered solutions corresponding to one of the individual sensors used for constructing the calibration line. All measurements were performed using the on-chip reference (Ag/AgCl/Nafion) and counter electrodes.

It is satisfying that these sensor devices then showed the expected pH response when operated in phosphate buffered solutions of varying pH values, Fig. 3. The observed SWV peak potentials for MB were found to vary linearly with pH of the solution in the range between 4.6−7.9, with a slope of and −52±3 −56±2 mV/pH for the forward and reverse SWV measurements carried out, corresponding to the oxidation and reduction of MB, respectively. This slope is comparable to the performance registered for the macro-SPAuEs in Fig 1D, whilst the change in intercept reflects the expected sign and magnitude of the systematic shift in the methylene blue SWV peak potentials for this Nafion/t-MB/Au/Pt electrode system as a result of using the on-chip reference electrode in this different chloride concentration along with the on-chip counter electrode.

3.3. Measurement of tissue pH *in vivo*

To test the efficacy of the Nafion/t-MB/Au/Pt pH sensor system developed above for measuring *in vivo* tissue pH changes the functionalised, packaged and calibrated sensing devices were implanted in an ovine pulmonary adenocarcinoma (OPA) tumour model. The sensor packaging was similar to that used in our previous work on oxygen sensing (Marland et al., 2020). All the sensor materials that were in direct contact with tissue have well-established biocompatibility profiles, while on the sensor, silicon dioxide (Kotzar et al., 2002; Voskerician et al., 2003; Stensaas and Stensaas, 1978) and Nafion (Lee et al., 2017; Kim et al., 2012; Turner et al., 1991) was exposed on the sensor surface. Both materials are well tolerated in biological systems, producing minimal foreign body response when implanted *in vivo*. The sensor was packaged in Epotek OG116–31 epoxy resin, which has been tested for compliance being an ISO 10993 biocompatibility standard. Connection to external instrumentation was made through a flexible circuit board manufactured from polyimide, which is commonly used for encapsulation and insulating implantable medical devices (Teo et al., 2016). Most previous biocompatibility studies on these materials used animal models involving implantation into healthy, non-diseased tissue. However, we have additionally previously reported that they do not cause changes in tumour pathology when implanted

within a solid tumour (Gray et al., 2019c)– an important consideration when sensors are deployed within the tumour microenvironment.

Following implantation into the lung tumour, changes in arterial blood pH, which is known to correlate with normal lung tissue pH (Effros and Chinard, 1969), were externally induced by mechanical ventilation (Section 2.10). Although lung tumour pH is also affected by other factors such as the metabolic activity of the tumour, it is known that it can be influenced by arterial blood changes such as bicarbonate content (Corbert and Feron, 2017), and here we used single-point arterial blood pH values taken throughout the experiment as means of assessing the ability of the implanted sensors to report on the externally-induced pH changes within the tumour.

A total of 4 implantation experiments were carried out in 3 sheep. The devices were implanted into a lung tumour as described in Section 2.9. The first implantation experiment (device-1 in Sheep Model-1, SM-1) enabled validation of the implantation/measurement methodology; whereas device-2 in SM-2 and devices-3 and 4 in SM-3 allowed pH tissue interrogation under externally-induced changes achieved via hyperventilation through the mechanical ventilation system or by including CO_2 in the administered gas mixture. A picture of the implanted device and measurement set-up is shown in Fig. 4A.

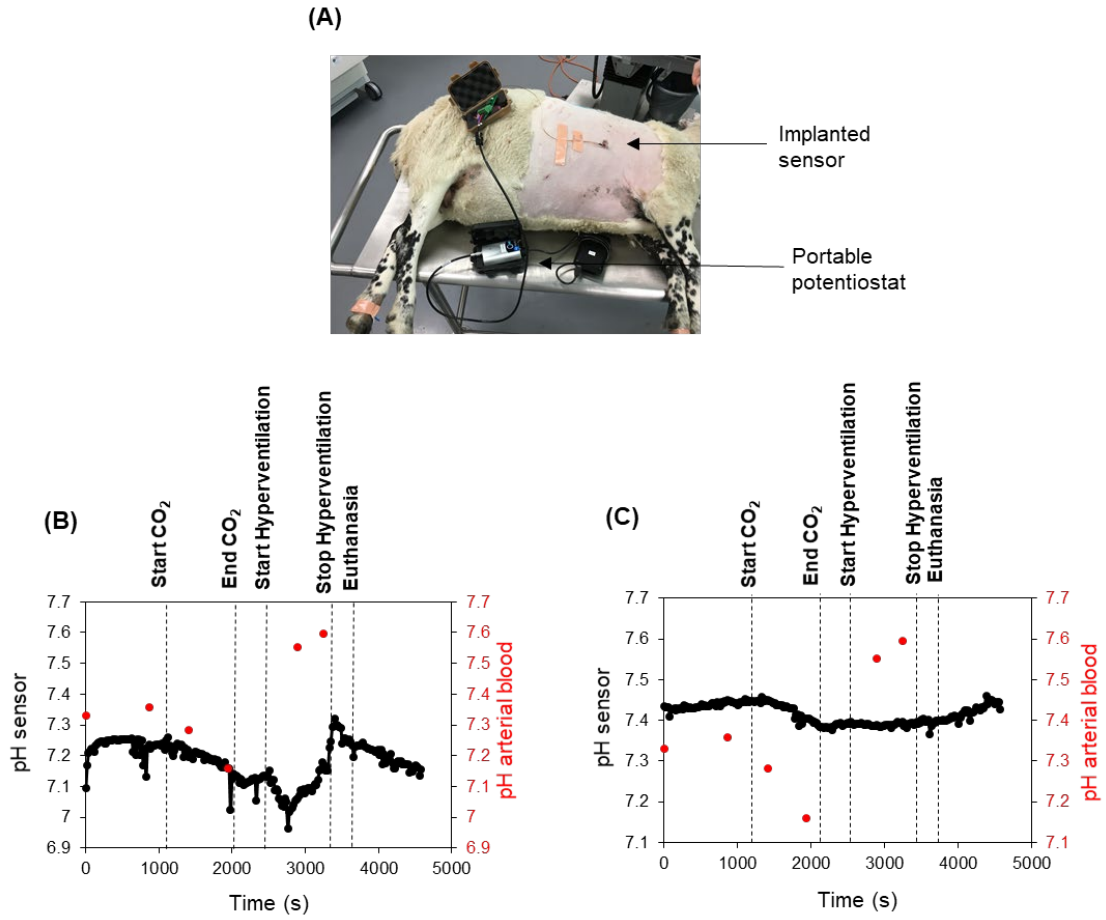

Figure 4. Monitoring pH changes *in vivo*. (A) Set up for performing implanted electrochemical measurements. The pH device is implanted and connected to the portable potentiostat during the measurements. (B) Calculated pH values from the peak potential registered for each individual device for the implanted experiments for device-3 in SM-3 and (C) device-4 in SM-3. Red dots represent single point arterial blood pH values taken during the experiment. External events are marked with a dotted line. All measurements were performed with the self-contained implanted device.

The first implanted device (device-1) allowed recording of the MB redox process continuously for a period of 30 min. For this experiment a 50 µm 3 x 3 Pt disc array was employed (see Supplementary Fig. 14 for picture of the device).The electrochemical signal recorded for the implanted sensor for both forward and reverse SWV are shown in

Supplementary Fig. 15 and the corresponding calculated pH is shown in Supplementary Fig. 16 (see Supplementary Fig. 17 for calibration lines). After implantation SM-1 was mechanically ventilated with an inspired fraction of oxygen of 0.5 that was increased to 1.0 after approximately 1000 s (for clinical needs during the procedure as a result of poor oxygen saturation). As shown in Supplementary Fig. 16, the pH calculated through the sensor's output decreased by 0.6 pH units during the first 10 min after implantation and remained stable afterwards until the failure of the device after 30 min of continuous operation. The arterial blood analysis showed a slight increase of 0.1 pH units. The sensor's output however, did not show an increase in the calculated pH, although this could be due to the small change inferred by the increase in oxygen. The malfunction of the device appeared as an uncontrolled redox potential. The continued functionality of device-1 after implantation was assessed by extraction and subsequent SWV experiments in PBS with the functionalised Nafion/t-MB/Au/Pt electrode system as working electrode and using external reference and counter electrodes. The fact that the sensor's modified working electrode was still able to report a signal corresponding to the redox process of MB even after being extracted post mortem showed that the active Nafion-coated SAM layer was able to withstand the entire implantation/measurement/extraction protocol. This was additionally supported by a subsequent Nafion integrity test that showed the continued ability of the Nafion layer to completely exclude a redox active anion (1 mM ferrocyanide) in solution (Supplementary Fig. 18). This confirms that the failure of the on-chip Ag/AgCl RE is behind the limited operating time of device-1 when implanted.

The second implanted device, device-2 in SM-2, also registered a decrease of the measured pH during the initial 400 s, as already seen for device-1, although in this case the change was smaller, at 0.05 pH units. After 1400 s of recording with a fixed gas mixture, CO_2 was administered. As shown in Supplementary Fig. 19, as expected this caused respiratory acidosis and a decrease in arterial blood pH. It was satisfying that not only the same decrease was observed for the implanted device, but that it was also the same magnitude as

the arterial blood measurement, of 0.2 pH units, which demonstrates the ability of the implanted device to track pH changes *in vivo*. After CO_2 administration was discontinued, both measured arterial blood pH and calculated pH values from device-2 increased, by 0.1 and 0.02 units, respectively. A further increase in the measured arterial blood pH was registered during subsequent mechanical hyperventilation, however, in this case the calculated pH from the sensor did not suffer changes. This lack or decrease on the sensor response that appeared with time of implantation could be explained by a loss of sensitivity experienced by the implanted devices, evident through post mortem examination (Supplementary Fig. 20), probably due to biofouling on the Nafion layer. Upon euthanasia, the output pH registered a sharp increase followed by a continuous decrease until the end of the experiment, in agreement with the expected pH decrease triggered by euthanasia due to loss of buffering and accumulation of lactic acid (Donaldson and Lamont, 2013). Peak potentials and peak currents registered for both forward and reverse SWV are depicted in Supplementary Fig. 21, and the administered CO_2 and O_2 values are summarised in Supplementary Table 1.

For the last experiment, two devices (device-3 and 4) were implanted in SM-3 in order to track the induced pH changes in two different anatomical locations in the same lung tumour. Fig. 4 shows the calculated pH values for device-3 and 4. In this case, the equilibration period after the onset of continuous measurement gave an increase of calculated pH of 0.15 units for device-3 and a fairly constant pH value for device-4. Afterwards, the pH was externally manipulated as previously described for SM-2. CO_2 administration caused a decrease of 0.2 pH units on the arterial blood pH, whilst both implanted devices registered a decrease in the measured pH upon CO_2 administration of 0.12 pH units for device-3, and 0.08 pH units for device-4. This variation in the sensors' response can be due to different tumour locations being affected differently in terms of pH changes. Subsequently, a hyperventilation period was applied, causing an increase of 0.44 pH units on the arterial blood pH. This change was detected by device-3, showing an increase of 0.16 units in pH

but not by device-4, whose signal remained invariable. In this case it is possible that both effects of different tumour locations and loss of sensitivity with time are affecting the sensors performance. After euthanasia, both implanted devices registered a clear pH change, but in opposite directions, decreasing by 0.1 pH units for device-3 and increasing by around 0.05 pH units for device-4. Peak potentials and peak currents registered for both forward and reverse SWV for devices 3 and 4 are depicted in Fig. 5 and Supplementary Fig. 22, respectively. The administered CO_2 and O_2 values corresponding to the experiment are summarised in Supplementary Table 2.

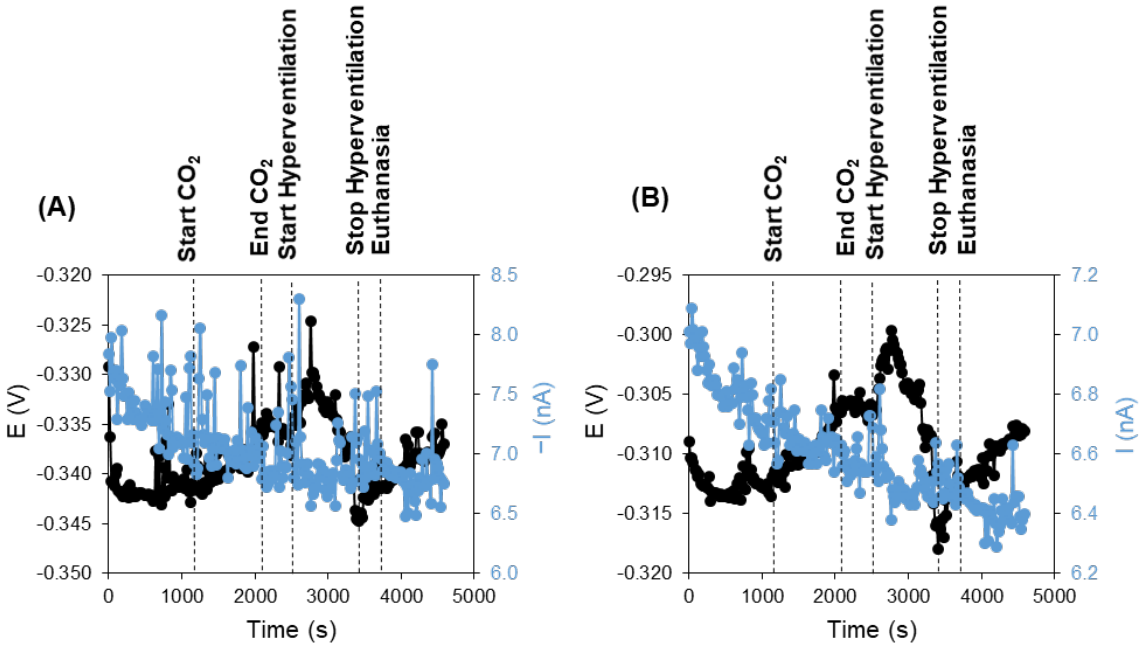

Figure 5. Electrochemical output registered for implanted sensors. (A) Electrochemical output registered for device-3 in SM-3 for the reverse and (B) forward measurements performed by SWV, corresponding to reduction and oxidation of MB, respectively. Black dots represent peak potentials and blue dots represent peak currents. All potentials are referred to the on-chip Ag/AgCl/Nafion reference electrode. Peak potential values were used to obtain the sensor's output calculated pH shown in Fig. 4A, using calibration lines shown in Fig. 3A and 3B.

Comparing the voltammograms corresponding to the first and last measurements performed for devices-2, 3 and 4 when implanted shows how the redox processes corresponding to the MB registered no big changes, with almost no decrease in peak currents (Supplementary Fig. 23). Post mortem recovered devices 2, 3 and 4 were found to maintain their pH activity, although with reduced sensitivity, as shown when pre- and post-implantation calibration lines are compared (Supplementary Fig. 20). All 3 devices showed no failure of the on-chip Ag/AgCl reference electrode during the 80 min experiment, as opposed to device-1. The reduced sensitivity registered after implantation is thought to be associated with tissue biofouling, and can explain the lower degree of response against induced pH changes observed at the end of each individual implanted experiment. The protective Nafion layer was still in place after implantation, as shown by the integrity test (Supplementary Fig. 24). Throughout the *in vivo* studies described above, we compared the tumour tissue pH measurements from our sensor to those of arterial blood pH measured using an external analysis system. This approach proved to be very useful, allowing us to confirm the efficacy of the various interventions, and providing a point of comparison for initial validation of sensor performance. However, it is likely that small pH differences will exist between blood and tissue, and between different locations within tissue. This may partly account for the variability observed in our results. To avoid these problems, the *in vivo* model could be refined in the future by co-implanting a calibrated commercial fibre-optic pH sensor alongside the electrochemical sensor (Correia et al., 2018). This would enable a more detailed assessment of sensor performance.

4. Conclusion

In conclusion, we have demonstrated the fabrication, optimisation and characterisation of an *in vitro* implantable, miniaturised electrochemical pH sensor. We validated its ability to operate *in vivo*, in an ovine lung tumour model. The sensor showed good sensitivity (−56±2

mV/pH unit) *in vitro* in the 4.6–7.9 range, as well as good reproducibility and repeatability was able to report on externally-induced pH tissue changes when implanted in vivo. The devices were operated continuously *in vivo* for 80 min without failure showing their robustness. Further work will integrate anti-biofouling coatings, in order to prevent loss of sensitivity following implantation, as observed through post-implantation tests.

References

Arifuzzaman, M., Millhouse, P.W., Raval, Y., Pace, T.B., Behrend, C.J., Behbahani, S.B., DesJardins, J.D., Tzeng, T-R. J., Anker, J.N., 2019. Analyst 144, 2984–2993.

Choudhary, T. R., Tanner, M.G., Megia-Fernandez, A., Harrington, K., Wood, H.A., Marshall, A., Zhu, P., Chankeshwara, S.V., Choudhury, D., Monro, G., Uncucu, M., Yu, F., Duncan, R.R., Thomson, R.R., Dhaliwal, K., Bradley, M., 2019. Sci. Rep. 9, 7713.

Cobo, A., Sheybani, R., Tu, H., Meng, E., 2016. Sensor. Actuat. A-Phys. 239, 18–25.

Corbert, C., Feron, O., 2017. Nat. Rev. Cancer 17, 577–593.

Correia, R., James, S., Lee, S-W., Morgan, S.P., Korposh, S., 2018. J. Opt. 20, 073003.

Cousens, C., Scott, P. R., 2015. Vet. Rec. 177, 366–366.

Donaldson, A. E., Lamont, I. L., 2013. PLoS One 8, e82011–e82021.

Douthwaite, M., Koutsos, E., Yates, D. C., Mitcheson, P. D., Georgiou, P., 2017. IEEE Trans. Biomed. Circuits Syst. 11, 1324–1334.

Edwards, C. A., Kouzani, A., Lee, K. H., Ross, E. K., 2017. Mayo Clin. Proc. 92, 1427–1444.

Effros, M. R., Chinard, F. P., 1969. J. Clin. Investig. 48, 1983–1996.

Gallagher, F. A., Kettunen, M.I., Day, S.E., Hu, D-H., Ardenjaer-Larsen, J.H., in 't Zandt, R., Jensen, P.R., Karlsson, M., Golman, K., Lerche, M.H., Brindle, K.M., 2008. Nature 453, 940–943.

García-Guzmán, J.J., Pérez-Rafols, C., Cuartero, M., Crespo, G.A., 2021. ACS Sens. 6, 1129–1137.

Giagkoulovits, C., Cheah, B. C., Al-Rawhani, M. A., Accarino, C., Busche, C., Grant, J.P., Cumming, D.R.S., 2018. IEEE Trans. Circuits Syst. I 65, 2821–2831.

Gong, Q., Wang, Y., Yang, H., 2017. Biosens. Bioelectron. 89, 565–569.

González-Fernández, E., Staderini, M., Yussof, A., Scholefield, E., Murray, A.F., Mount, A.R., Bradley, M., 2018. Biosen. Bioelectron. 119, 209–214.

Grant, S. A., Bettencourt, K., Krulevitch, P., Hamilton, J., Glass, R., 2001. Sensor. Actuat. B-Chem. 72, 174–179.

Gray, M., Meehan, J., Ward, C., Langdon, S.P., Kunkler, I.H., Murray, A., Argyle, D., 2018. Vet. J. 239, 21–29.

Gray, M.E., Marland, J.R.K., Dunare, C., Blair, E.O., Meehan, J., Tsiamis, A., Kunkler, I.H., Murray, A.F., Argyle, D., Dyson, A., Singer, M., Potter, M.A., 2019. Am. J. Physiol. Gastrointest. Liver Physiol. 317, G242–G252.

Gray, M. E., Sullivan, P., Marland, J.R.K., Greenhalgh, S.N., Meehan, J., Gregson, R., Clutton, E.E., Cousens, C., Griffiths, D.J., Murray, A, Argyle, D., 2019. Front. Oncol. 9, 335.

Gray, M. E., Meehan, J., Blair, E. O., Ward, C., Langdon, S. P., Morrison, L. R., Marland, J., Tsiamis, A., Kunkler, I. H., Murray, A., Argyle, D., 2019. J. Biomed. Mater. Res. B 107(5), 1620–1633.

Gu, Z., Liu, H-X., Ying, Y-L., Xiu, G., Long, Y-T., 2018. Analyst 143, 2760–2764.

Hammond, P. A., Ali, D., Cumming, D. R. S., 2004. IEEE Sensors J. 4, 706–412.

Inmann, A., Hodgins, D., 2013. Implantable Sensors Systems for Medical Applications Woodhead Publishing, Oxford.

Ju, H., Zhou, J., Cai, C., Chen, H., 1995. Electroanal. 7, 1165–1170.

Ju, H., Xun, Y., Chen, H., 1995. J. Electroanal. Chem. 380, 283–285.

Kelley, S. O., Barton, J. K., Jackson, N. M., Hill, M. G., 1997. Bioconjugate Chem. 8, 31–37.

Kim, G., Kim, H., Kim, I.J., Kim, J.R., Lee, J.I., Ree, M., 2012. J. Biomater. Sci. Polym. Ed. 20, 1687–1707.

Kotzar, G., Freas, M., Abel, P., Fleischman, A., Roy, S., Zorman, C., Moran, J.M., Melzak, J., 2002. Biomaterials 23(13), 2737–2750.

Koutsoumpeli, E., Murray, J., Langford, D., Bon, R. S., Johnson, S., 2015. Sens. Biosensing Res. 6, 1–6.

Lee, Y.J., Kim, H.-J., Kang, J.Y., Do, S.H., Lee, S.H., 2017. Adv. Healthc. Mater. 6, 1–12.

Love, J. C., Estroff, L. A., Kriebel, J. K., Nuzzo, R. G., Whitesides, G. M., 2005.Chem. Rev.105, 1103–1170.

Marland, J.R.K., Gray, M.E., Dunare, C., Blair, E.O., Tsiamis, A., Sullivan, P., González-Fernández, E., Greenhalgh, S.N., Gregson, R., Clutton, R.E., Parys, M.M., Dyson, A., Singer, M., Kunkler, I.H., Potter, M.A., Mitra, S., Terry, J.G., Smith, S., Mount, A.R., Underwood, I., Walton, A.J., Argyle, D.J., Murray, A.F., 2020. Sens. Biosensing Res. 30, 100375−100386.

Nakata, S., Arie, T., Akita, S., Takei, K., 2017. ACS Sens. 2, 443−448.

Rudnev, A. V., Zhumaev, U., Utsunomiya, T., Fan, C., Yokota, Y., Fukui, K., Wandlowski, T., 2013. Electrochim. Acta 107, 33–44.

Scholten, K., Meng, E., 2018. Int. J. Pharm. 544, 319−334.

Scott, P. R., Dagleish, M. P., Cousens, C., 2018. Ir. Vet. J. 71, 23–31.

Staderini, M., González-Fernández, E., Murray, A. F., Mount, A. R., Bradley, M., 2018. Sensors, Sensor. Actuat. B-Chem. 274, 662–667.

Stensaas, S.S., Stensaas, L.J., 1978. Acta Neuropathol. 41, 145-155.

Stine, K. J., 2019. Appl. Sci. 9, 797–837.

Swietach, P., Vaughan-Jones, R. D., Harris, A. L., Hulikova, A., 2014. Phil. Trans. R. Soc. B 369, 20130099–20130108.

Teo, A.J.T., Mishra, A., Park, I., Kim, Y.-J., Park, W.-T., Yoon, Y.-J., 2016. ACS Biomater. Sci. Eng. 2, 454–472.

Terry J.G., Schmüser, I., Underwood, I., Corrigan, D.K., Freeman, N.J., Bunting, A.S., Mount, A.R., Walton, A.J., 2013. IET Nanobiotechnol. 7, 125–134.

Tsai, Y-C., Li, S-C., Chen, J-M., 2005. Langmuir 21, 3653–3658.

Turner, R.F.B., Harrison, D.J., Rojotte, R.V., 1991. Biomaterials 12, 361–368.

Verma, N., Knight, B. P., 2019. Arrhythm. Electrophisiol. Rev. 8, 228–233.

Voskerician, G., Shive, M.S., Shawgo, R.S., von Recum, H., Anderson, J.M., Cima, M.J., Langer, R., 2003. Biomaterials 24(11), 1959–1967.

Wang, L., Xie, S., Wang, Z., Liu, F., Yang, Y., Tang, C., Wu, C., Liu, P., Li, Y., Saiyin, H., Zheng, S., Sun, X., Xu, F., Yu, H., Peng, H., 2020. Nat. Biomed. Eng. 4, 159–171.

Wilson, B.S., Finley, C.C., Lawson, D.T., Wolford, R.D., Eddington, D.K., Rabinowitz, W.M., 1991. Nature 352, 236–238.

Acknowledgements

The authors acknowledge financial support from the EPSRC-funded Implantable Microsystems for Personalised Anti-Cancer Therapy (IMPACT) programme [Grant re. EP/K034510/1] and from a Wellcome Trust Biomedical Resource Grant to the Wellcome Trust Critical Care Laboratory for Large Animals (104972/Z/14/Z). J. Nixon, P. Tennant and A. Ritchie for sheep husbandry and sensor sterilisation, and L. Grant for CT imaging. Sheep OPA cases were obtained by P. Scott (Capital Veterinary Services). A.U. acknowledges the doctoral scholarship from the Republic of Turkey, Ministry of National Education through the YLSY programme.

Author contributions

EG-F, ARM & MB conceived the electrochemical sensing approach for pH. MS synthesised all probes. JRKM, CD, EOB, AT & EG-F designed and fabricated the in-house sensors. EOB developed the packaging procedure and carried out packaging for all implanted sensors. EG-F performed all development and characterisation experiments. MEG, PS, SNG, RG, REC & DJA developed methodology for the lung tumour implantation experiments and MEG, PS, JRKM, EG-F and AU performed the sheep *in vivo* work. EG-F analysed the data, with input from AU, JRKM and MEG for *in vivo* data analysis. AFM, ARM, MB, DJA, AJW, SS, JGT, SNG & REC supervised the experiments. EG-F wrote the manuscript with input from MS for synthetic methods, JRKM for in-house fabrication and MEG for implantation protocol. The manuscript was reviewed and edited by all the authors.

Competing interests

The authors declare no competing interests.